Orbital-dependent electron dynamics in Fe-pnictide superconductors

Ganesh Adhikary,[1,*] Barbara Ressel,[1] Matija Stupar,[1] Primož Rebernik Ribič,[2] Jurij Urbančič,[1] Giovanni De Ninno,[1,2,†] D. Krizmancic,[3] A. Thamizhavel,[4] and Kalobaran Maiti[4,‡]

[1]*Laboratory of Quantum Optics, University of Nova Gorica, 5001 Nova Gorica, Slovenia*

[2]*Elettra-Sincrotrone Trieste, Area Science Park, 34149 Trieste, Italy*

[3]*Laboratorio TASC, IOM-CNR, SS 14 km 163.5, Basovizza, 34149 Trieste, Italy*

[4]*Department of Condensed Matter Physics and Materials' Science, Tata Institute of Fundamental Research, Homi Bhabha Road, Colaba, Mumbai 400 005, India*

(Received 20 November 2017; revised manuscript received 25 August 2018; published 21 November 2018)

We report on orbital-dependent quasiparticle dynamics in $EuFe_2As_2$, a parent compound of Fe-based superconductors, and a way to experimentally identify this behavior using time- and angle-resolved photoelectron spectroscopy across the spin density wave transition. We observe two different relaxation timescales for photoexcited d_{xz}/d_{yz} and d_{xy} electrons. While the itinerant d_{xz}/d_{yz} electrons relax faster through the electron-electron scattering channel, d_{xy} electrons form a quasiequilibrium state with the lattice due to their localized character, and the state decays slowly. Our findings suggest that electron correlation in Fe pnictides is an important property, which should carefully be taken into account when describing the electronic properties of both parent and carrier-doped compounds, and therefore establish a strong connection with cuprates.

DOI: 10.1103/PhysRevB.98.205142

I. INTRODUCTION

Electron correlation plays a key role in the mechanism of high-temperature superconductivity in cuprates [1,2]. Strong electron correlation is, indeed, responsible for both Mott behavior of parent compounds and high-T_c superconductivity upon electron or hole doping [3]. Since the discovery of high-T_c superconductivity in Fe pnictides [4,5], extensive research has been carried out to understand the pairing mechanism in these systems [6]. While several studies point to the existence of strongly correlated electrons in the presence of hole doping [7], electron correlation has hardly been detected in parent and electron-doped compounds [8–11].

One of the complicating factors in Fe-based compounds is that multiple bands (or orbitals) form the Fermi surface, which makes these systems more complex than cuprates, where the contribution to the Fermi surface comes only from the $d_{x^2-y^2}$ orbital [3,6]. In Ref. [12], de' Medici *et al.* proposed orbital-selective Mottness as an explanation of the unconventional properties of Fe-based superconductors. Each orbital shows single-band Mott behavior, where the degree of electron correlation depends on the doping of the bands from half filling. Such orbital decoupling and differentiation of correlation strength among different orbitals are caused by Hund's rule that prevents interorbital coupling. The theory is also supported by recent results obtained for LiFeAs [13] and several Fe-chalcogenide systems using angle-resolved photoemission spectroscopy (ARPES), for which it was shown that $3d_{xy}$ electrons are localized, whereas those associated with other $3d$ orbitals are itinerant [14] in nature. Additional evidence for orbital-selective Mott phase behavior in Fe-chalcogenide systems comes from terahertz spectroscopy [15], Hall measurements [16], pump-probe spectroscopy [17], and high-pressure transport measurements [18]. Theoretical calculations within the multiorbital Hubbard model on $K_{1-x}Fe_{2-y}Se_2$ also supports this picture [19].

However, for Fe pnictides, different experiments and theory show that the differentiation of the correlation strength among orbitals is low for the parent compound and decreases further with electron doping [12,20]. Since superconductivity emerges even in electron-doped compounds where all the electrons appear to be itinerant, this raises the question of whether strong electron correlation is really the key ingredient required to explain the unconventional properties of the Fe-pnictide family.

Recently, several time-resolved pump-probe experiments were carried out in order to study optically excited states in Fe pnictides [21–23] and gain further understanding of the electronic properties of these systems. For instance, pump-probe data on superconducting $Ba_{1-x}K_xFe_2As_2$ samples [22] revealed fast- and slow-relaxation timescales for photoexcited carriers, which were associated, respectively, with recombination of quasiparticles through interband and intraband processes. The pump-probe data for $EuFe_2As_2$ exhibit a reformation timescale for magnetic order slower than electron-phonon equilibration timescale [23]. These studies were not able to disentangle the role played by different orbitals but confirmed that the electronic properties of these systems stem from the multiband nature of the Fermi surface.

In this paper, we propose an orbital-selective method allowing us to study the relaxation dynamics of photoexcited electrons near the Fermi level and use it as a powerful tool to gain deep insight into electron localization in Fe pnictides.

*Corresponding author: ganesh.adhikary@ung.si

†Corresponding author: giovanni.de.ninno@ung.si

‡Corresponding author: kbmaiti@tifr.res.in

In essence, by using time- and angle-resolved photoelectron spectroscopy (trARPES) on $EuFe_2As_2$, a parent compound of the Fe-pnictide family, we observe two different relaxation timescales for electrons in d_{xz}/d_{yz} and d_{xy} orbitals, selectively probed by adjusting the polarization of the pump laser [3]. The slow- (fast-) relaxation dynamics of excited d_{xy} (d_{xz}/d_{yz}) electrons is associated with their localized (itinerant) nature. Our results demonstrate that the differentiation of the correlation strength among orbitals in Fe pnictides might be higher than previously thought.

II. EXPERIMENT

The electronic structure of Fe-based superconductors typically consists of three hole bands at the Brillouin zone center (Γ point) and two electron bands at the Brillouin zone corner (M point); the number of distinct hole/electron bands may vary depending on the degeneracy of the involved electronic eigenstates. In order to get an overview of the electronic structure of $EuFe_2As_2$, we calculated the electronic band structure employing the *state-of-the-art* full-potential linearized augmented-plane wave method within the local-density approximation using WIEN2K software [24]. We used experimentally found lattice constants, $a = b = 3.9$ Å and $c = 12.1$ Å for the paramagnetic tetragonal structure (space group $I4/mmm$), and the convergence was achieved with tolerance in energy < 1 meV per formula unit.

The calculated energy bands shown in Fig. 1(a) exhibit three hole pockets around the Γ point denoted by α, β, and γ (energy band dispersion in a larger energy range is given in the Appendix). The electron pockets around the M point are denoted by ξ and ε. The inner electron pocket denoted by ϵ at the M point exhibits a nesting condition with the β band [25]. It is well established that this nesting between the electron pocket ε and the hole pockets formed by the β band causes the spin density wave (SDW) transition in these compounds [26]. In Fig. 1(b), we show the schematic of the surface Brillouin zone for (001) plane along with the nesting vector Q_N. The schematic exhibiting the opening of the SDW gap below the Néel temperature, 190 K, due to the nesting of the β and ε bands is shown in Fig. 1(c).

The partial densities of states of d_{xy} and degenerate (d_{xz}/d_{yz}) states are shown in Fig. 1(d); the width of the d_{xy} band is significantly narrower than the width of the other bands. This indicates that the effective electron correlation strength U/W (U is the electron-electron Coulomb repulsion strength, and W is the bare bandwidth) will be relatively stronger for the d_{xy} electrons than the others even if we consider U to be the same for all d electrons. Usually, U increases with the narrowing of the bands, which makes the trend of change in U/W even stronger. Such orbital dependence of the correlation-induced effect was shown theoretically in similar systems [12,27].

ARPES is the tool of choice for probing the electronic structure of a system directly. In a trARPES experiment, the dynamics of photoexcited electrons can be tracked by varying the time delay Δt between a low-energy (visible or infrared) pump and a high-energy (extreme ultraviolet) probe beam. This gives information about different coupling phenomena, excitation modes, and relaxation processes. As we demonstrate below, by adjusting the polarization of the excitation pulse, electronic states can be probed selectively. In Figs. 2(a) and 2(c), we show the experimental geometry for the two configurations when the pump is either s polarized (s-pol) or p polarized (p-pol). The electric dipole moment vector in the s-pol case is in the plane of the sample surface, whereas the dipole vector for the p-pol beam makes an angle of 36° with the sample surface normal. In the s-pol configuration, the pump beam excites the electrons with d_{xy} and d_{yz} symmetry as the electric dipole moment vector has a finite component along the orbital lobe of both these orbitals, as shown in Fig. 2(b) and 2(d), respectively; it has no component for d_{xz} states. On the other hand, the p-pol configuration of the pump beam will excite predominantly d_{xz} states [see Fig. 2(d)] [28–30].

Time- and angle-resolved photoemission spectroscopy was carried out using a mode-locked Ti:sapphire laser system delivering pulses at 1.5 eV (800 nm), with a 50-fs duration

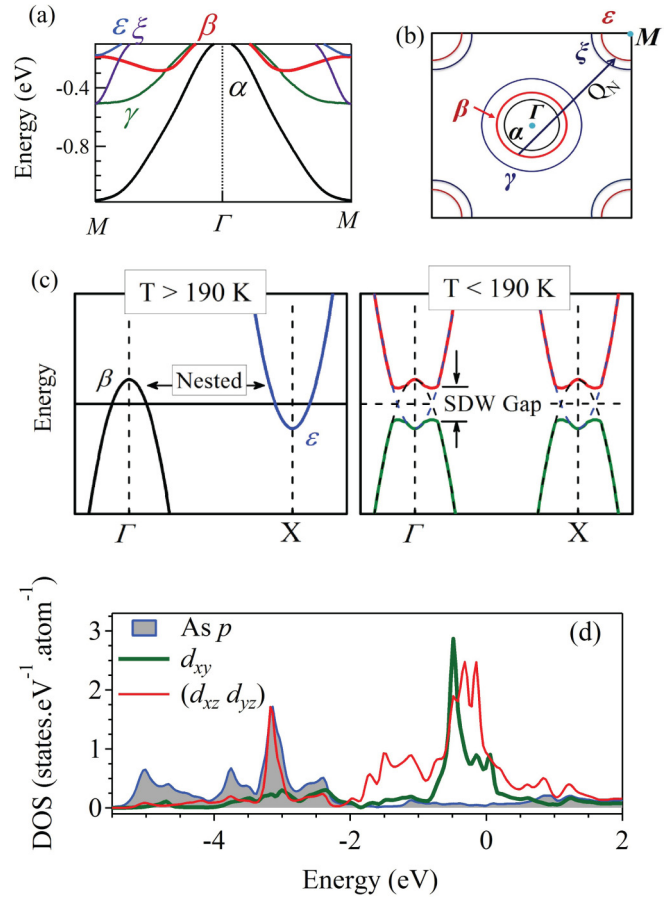

FIG. 1. (a) Calculated energy bands of $EuFe_2As_2$ along the $M\Gamma M$ direction exhibiting α, β, and γ bands forming the hole pockets around the Γ point and ε and ξ bands forming electron pockets around the M point. (b) Schematic of the surface Brillouin zone showing the three hole pockets around Γ and two electron pockets around M. The nesting vector Q_N for the SDW phase is also shown. (c) Schematic showing the opening of the SDW gap below 190 K due to the nesting of β and ε bands. (d) Partial densities of states of d_{xy} (thick green line) and degenerate d_{xz}/d_{yz} states (red line). As p states are shown by an area plot.

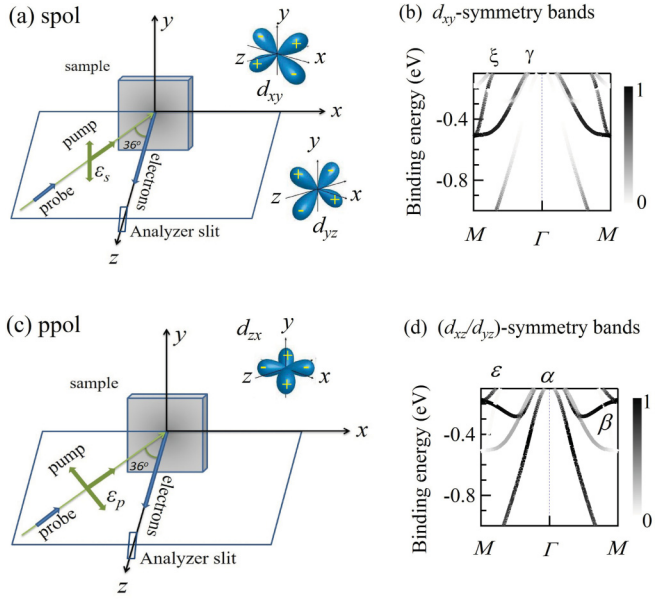

FIG. 2. (a) Schematic of the experimental geometry for the excitation by s-polarized pump pulse and the orientation of d_{xy} and d_{yz} orbitals in a similar axis system. (b) Calculated energy bands emphasizing d_{xy} symmetry. (c) Experimental geometry for the p-polarized pump-pulse excitations and the orientation of the d_{xz} orbital. (d) Calculated energy bands emphasizing d_{xz}/d_{yz} symmetry.

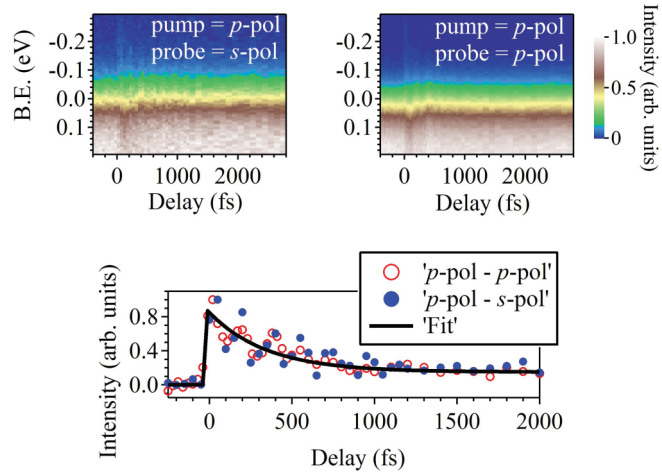

FIG. 3. Decay of the electronic states after excitation by the p-polarized pump pulse and probing by the s-polarized (top left panel) and p-polarized (top right panel) probe pulse. The k-integrated data in the energy range of -0.1 to -0.2 eV are shown in the bottom panel. The black solid line represents the fit of the experimental data; both cases show similar decay dynamics.

and 5-kHz repetition rate. The pulse was split into two parts. The major part of the intensity was used to produce high-order harmonics, spanning the energy range from 10 to 50 eV, using argon as the generating medium [31]. The second part of the beam was used as a pump whose intensity was controlled with a variable attenuator based on a half-wave plate and a polarizer. We could select the desired harmonics and control their flux by means of a specially designed grating setup, which preserves the pulse duration. The probe energy was set to 29 eV. The use of this relatively high photon energy enables probing a larger k range in the reciprocal space for a fixed acceptance angle of the electron analyzer. At lower photon energies, the photoionization cross section [32] of As $4p$ states is much higher than that of Fe $3d$ states, and the contribution from secondary electrons becomes significant. The photoemission chamber was equipped with an R3000 analyzer from VG Scienta, a five-axis manipulator, and a closed-cycle He cryostat from Prevac.

Single-crystalline $EuFe_2As_2$ samples were grown by the Sn-flux method and characterized by x-ray diffraction, Laue diffraction, and energy dispersive analysis of x rays [33]. The sample was cleaved *in situ* at a pressure of about 5×10^{-10} Torr to generate a clean and flat surface before each measurement. The measurements were done at 1×10^{-10} Torr. The static ARPES data were found to be of high quality (see the Appendix) and match well with the published literature [34].

III. RESULTS AND DISCUSSION

First, we investigate the influence of probe-pulse polarization on the trARPES spectral functions after an orbital-selected excitation is done using the polarized pump pulse. We excited $EuFe_2As_2$ using a p-polarized pump pulse as shown schematically in Fig. 2(c). The excited state is probed by both p-polarized and s-polarized probe pulses. The corresponding experimental data collected at 200 K are shown in Fig. 3. The top panel shows the k-integrated experimental data along the ΓM direction as a function of time delay between the pump pulse and the probe pulse. In order to probe the lifetime of the excited electrons (often termed hot electrons), we have integrated intensity in the energy range of 0.1–0.2 eV above the Fermi level, which is significantly away from the Fermi level and has little influence due to the Fermi-Dirac distribution function at 200 K (sample temperature). Results are shown in the bottom panel of Fig. 3 as a function of time delay. The decays of the hot electron intensity for both p-polarized and s-polarized cases superimpose well, indicating very similar decay dynamics in both cases.

We now investigate the effect of pump polarization on the trARPES spectral function obtained by the s-polarized probe pulse. In Fig. 4, we show the difference of the trARPES data collected at time delays of -300 and 200 fs. The integrated area in the regions denoted by the red and blue boxes is shown in Fig. 4(c); the blue box encloses the contribution from the γ band, and the red box encloses the (α, β) bands. We observe a significant difference between the blue and red curves for the case in which excitation is done using the p-polarized pump pulse. These experimental results indicate less influence of p-polarized light on the electronic states corresponding to the γ-band with d_{xy} symmetry compared to the excitation of α- and β-band states possessing d_{xz}/d_{yz} orbital symmetry. On the other hand, the s-polarized case shows similar intensities for both the red and blue boxes as the s-polarized light can excite both d_{yz} and d_{xy} states, as shown in Fig. 2(a).

In static photoemission spectroscopy, the spectral functions are derived by the final states of the photoexcitation process. In trARPES, the probe pulse probes the electronic states excited by the pump pulse, and the relationship between the

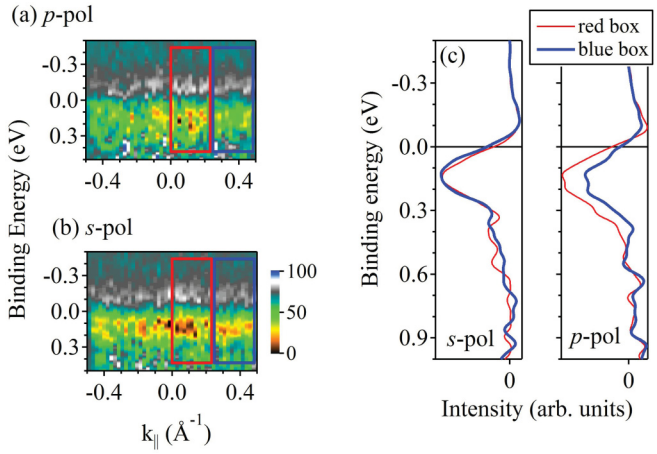

FIG. 4. Difference of the spectra collected at −300 and 200 fs time delay using (a) *p*-polarized and (b) *s*-polarized pump pulses. The integrated areas inside the red and blue boxes are shown in (c), which exhibits a distinct difference between the blue and red curves for the *p*-polarized case, while those for the *s*-polarized case appear similar.

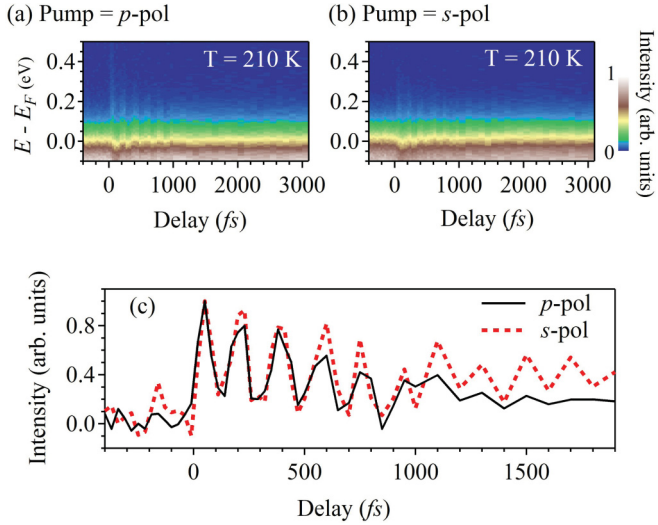

FIG. 5. Time-resolved photoemission spectra as a function of Δt at 210 K using (a) *p*-polarized (*p*-pol) and (b) *s*-polarized (*s*-pol) pump pulses. (c) Intensity of the hot electrons (integrated between 0.1 and 0.2 eV above the Fermi level) as a function of Δt for both pump polarizations. A significant difference in decay is observed for $\Delta t > 1$ ps.

polarization of the pump pulse and the probe pulse is not *a priori* clear. The scenario becomes even more complex as the Wannier functions often used to derive the electronic structure of solids do not vanish in different symmetry directions due to the hybridization of the electronic states involving atoms at different symmetry planes/sites. Thus, the derivation of the role of light polarization on the photoemission response calls for the development of suitable theoretical methods. However, the experimental observations discussed above provide evidence that the polarized pump pulse can be exploited to derive the orbital-selective behavior of the system. This is outstanding considering the fact that the valence band of most exotic materials is constituted by multiple bands and orbital-selective information is crucial to reveal the underlying physics of the exoticism of the material.

In Figs. 5(a) and 5(b), we show the time-resolved photoemission spectra as a function of the time delay Δt between the pump and probe pulses at 210 K ($T > T_N$) for both polarizations, *p*-pol and *s*-pol, respectively. The results show a sharp rise in intensity at $\Delta t = 0$ (corresponding to temporal overlap of the pump and probe pulses) followed by coherent oscillations and a decay of the signal in the picosecond timescale [see Fig. 5(c)]. Followed by the optical excitation of the electrons to the unoccupied states, electron-electron scattering and electron-lattice interactions give rise to different coherent collective excitation modes such as phonons and magnons within tens of femtoseconds. The frequency of oscillations is 5.6 THz (around 23 meV) for both polarizations, which corresponds to the fully symmetric A_{1g} phonon mode triggered by the breathing of As atoms along the *c* axis [35]. It is worth stressing that we have not observed a significant change in the electron dynamics with pump fluence within the range of 2–5 mJ/cm^2, as these pulse energies are far too low to excite the system into the anharmonic regime [36]. While coherent oscillations seem to be similar for both polarizations at lower Δt, we observe a significant difference in the electron relaxation dynamics for $\Delta t > 1$ ps; the intensity of the signal decreases faster in the *p*-pol configuration than in the *s*-pol case. Furthermore, the data in the *p*-pol configuration show faster damping of the oscillations.

The intensity of the hot electrons I_+ above and below T_N is shown in Fig. 6 for both *p*-pol and *s*-pol pump excitations. To analyze the temporal dynamics of the hot holes (I_-), we integrated the signal in a 100 meV energy window below the Fermi level. The time-dependent intensity profiles of the hot holes for *p* and *s* polarizations of the pump at different temperatures are shown in Fig. 7. We used $I_{+,-} = A\exp(-t/\tau_{+,-}) + B$ as a fit function, allowing us to extract the decay time constant of the excited states. Here, A is the amplitude of the excitation, $\tau_{+,-}$ are the decay time constants of the excited electrons and holes, respectively, and B accounts for the background originating from electron-phonon scattering. The fitting function was multiplied by a step function at $\Delta t = 0$ and convoluted with a Gaussian function to account for finite durations of the pump and probe pulses. The extracted decay constants vs temperature for hot electrons and holes are shown in Figs. 6(c) and 7(c), respectively for both polarizations. The hot-electron dynamics are significantly different for the two pump polarizations, as shown in Fig. 6(c). The decay is fast, with a time constant of approximately 500 fs, when pumped by *p*-pol light. For the *s*-pol pump pulse, the decay is slow, with a time constant in the range of 1–2 ps. Furthermore, the dynamics of hot electrons shows considerably (a factor of 3) slower relaxation in the SDW phase compared to high temperatures when pumped by *p*-pol, while for *s*-pol pumping, changes with temperature are not significant.

In the *p*-pol configuration, the pump beam primarily excites electrons in d_{xz} orbitals, as demonstrated in Fig. 2(c). Their fast-relaxation dynamics can be explained by strong

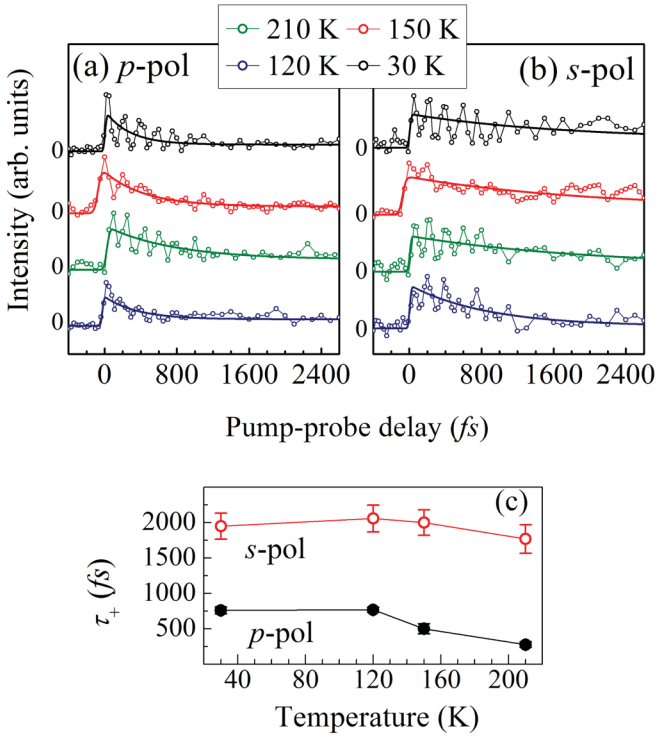

FIG. 6. Spectral intensity of the hot electrons as a function of Δt for (a) p-polarized and (b) s-polarized pump pulses at different sample temperatures. Solid lines represent single exponential fits. (c) Decay time constants of the hot electrons τ_+ as a function of temperature for p-pol and s-pol pump pulses. Significantly different time constants for p-pol and s-pol responses demonstrate successful polarization selection of different decay channels by the polarized pump pulse.

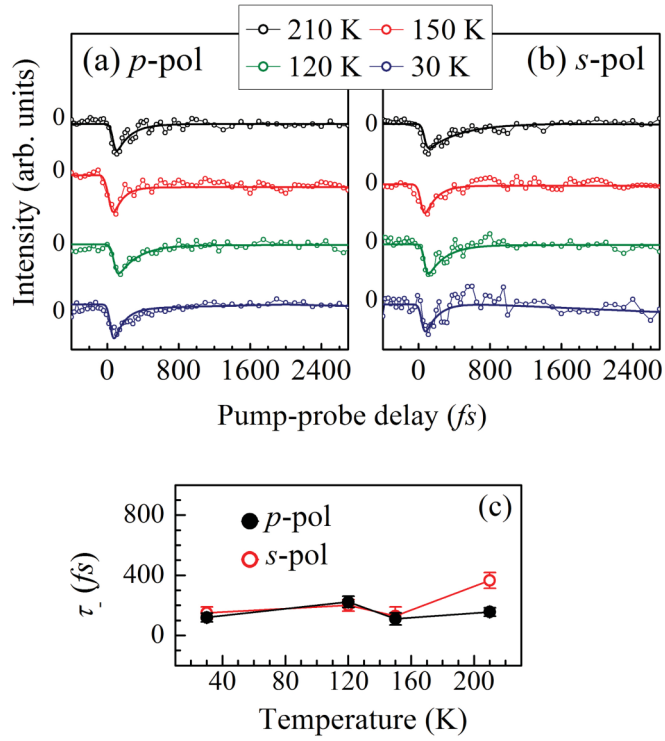

FIG. 7. Spectral intensity of hot holes as a function of Δt for (a) p-polarized and (b) s-polarized pump pulses at different sample temperatures. Solid lines represent single exponential fits. (c) Hole decay time constants τ_- for p-polarized and s-polarized pump pulses as a function of temperature. While the hole for s-pol case survives longer than the hole for p-pol case at 210 K, this difference in decay times becomes negligible in the SDW phase.

interband scattering between the β band and the electron pocket at the M point (ϵ band) [22], which is possible due to their good Fermi surface nesting. We argue that such fast-relaxation dynamics, i.e., the ability to efficiently dissipate energy, can be associated with the itinerant (delocalized) nature of d_{xz} electrons. On the other hand, the relaxation dynamics observed for s-polarized light is complex. At a short delay time, it seems to follow a trend akin to the p-pol case, but the difference becomes significant at longer delay; hot electrons survive for a much longer time in the s-pol case. As demonstrated in Fig. 2(a), the s-polarized pump pulse can excite both d_{yz} and d_{xy} states. Thus, the data in the shorter delay time seem to be influenced by the decay of d_{yz} states, while the longer delay time is predominantly contributed by the decay of d_{xy} states, which is almost absent in the p-pol case. As the γ band has no nesting condition with any other band, d_{xy} electrons can decay only through intraband scattering and hence are longer lived.

A similar scenario also manifests in the hole dynamics through the difference in decay time in the paramagnetic phase [210 K; see Fig. 7(c)], where the behaviors of the d_{xy} and d_{xz}/d_{yz} orbitals are significantly different. The decay of holes is primarily governed by the energy transfer to the lattice through electron-phonon relaxation. This is manifested by the somewhat faster relaxation of hot holes with decreasing temperature as more and more phonon modes are available for energy transfer at lower temperatures and thus enhances the phase space for electron-phonon scattering. The decay of d_{xz} holes is found to be less sensitive to temperature due to various competing effects such as opening of the SDW gap, nematicity (lifting the degeneracy of $d_{xz}d_{yz}$ bands), change in structural parameters, etc.

It should be noted here that it is possible to capture orbital-dependent behavior via the calculation of scattering rates of the polarization-dependent bands obtained from static ARPES [37,38]. The static ARPES spectral functions, derived by the final states of the photoemission process, reflect information of the relaxation of holes. The method proposed here probes the lifetime of the excited electrons due to the pump pulse in addition to the lifetime of the holes. This helped us to discover that the lifetime of the hot electrons is significantly different from that of the holes and reveals the differences in relaxation processes, which could not be captured from the lifetime of the holes.

We can obtain further insight into the electron relaxation dynamics by resorting to the Rothwarf-Taylor model [39]. According to the model, in a compound with an energy gap of 2Δ, the decay rate of the excited states depends on a number of processes. First, the recombination of the quasiparticles (QPs) across the SDW gap can take place. This process creates a photon of energy 2Δ. In the second step, the emitted photon can recreate another QP pair, create a low-energy boson (such

as a phonon), or escape out of the probed region. In the normal (non-SDW) phase, only the latter two processes can take place. On the other hand, when the system is brought into the SDW state, a gap opens up at the Fermi level in the β band. This generates a relaxation bottleneck due to QP recombination and recreation; that is, the QPs may form a quasiequilibrium state with the lattice, which we observe as an increase in the decay time constant at lower temperatures [Fig. 6(c)] in the case of the p-polarized pump. In the s-pol configuration, where the decay is primarily governed by the relaxation of d_{xy} electrons, we observe no significant change in the decay time constant as the γ band does not participate in the SDW transition.

IV. CONCLUSIONS

In summary, we have demonstrated a powerful method, complementary to the measurement of electron effective mass, allowing us to probe orbital-selective Mott phase behavior in strongly correlated materials. Specifically, we observed two different timescales for the relaxation of electrons in d_{xz}/d_{yz} and d_{xy} orbitals in $EuFe_2As_2$, a parent compound of Fe-based superconductors. We found that d_{xz}/d_{yz} electrons relax fast through electron-electron scattering. Such fast-relaxation dynamics can be attributed to the itinerant nature of these orbitals. On the other hand, d_{xy} electrons are found to relax over significantly longer timescales. We associate the slow dynamics to the fact that such electrons create a quasiequilibrium state with the lattice due to their high degree of localization. Although the ratios between effective masses of electrons belonging to d_{xz}/d_{yz} and d_{xy} orbitals measured with different techniques, such as ARPES and quantum oscillations, are $\sim$1 [40–42], our results show that the nature of electrons in these two types of orbitals is quite different. Our findings suggest that orbital-dependent electron correlation in Fe pnictide is important and should be carefully taken into account when describing the electronic properties of both parent and carrier-doped compounds and therefore establish a strong connection with the cuprates.

ACKNOWLEDGMENTS

K.M. acknowledges financial assistance from the Department of Science and Technology, government of India, under the J.C. Bose Fellowship program and the Department of Atomic Energy, government of India, under the DAE-SRC-OI Award.

APPENDIX

1. Band structure in extended energy scale

The energy band structure of $EuFe_2As_2$ was calculated employing the *state-of-the-art* full-potential linearized augmented plane-wave method within the local-density approximation using WIEN2K software [24] as discussed in Sec. II. In Fig. 8, we show the calculated energy bands along the $M\Gamma M$ direction in a wide energy scale; the k vector is the same as that used for ARPES measurements. We observe several weakly dispersive bands in the vicinity of the Fermi level appearing due to the partially filled Eu $4f$ contributions. While almost flat dispersion of these bands indicates strong local character, their energies could not be captured well due to

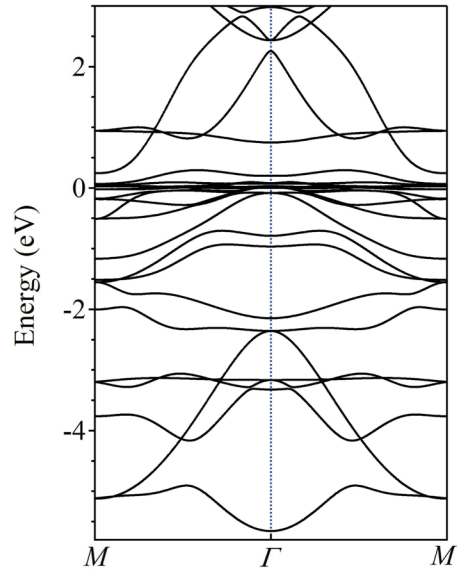

FIG. 8. Energy band structure of $EuFe_2As_2$ along the $M\Gamma M$ direction. The results are obtained by employing the full-potential linearized augmented plane-wave method.

the underestimation of the Coulomb repulsion strength among the $4f$ electrons (often termed electron correlation) in the effective single-particle density functional theory. Different theoretical approaches are required to estimate the Eu $4f$ energies correctly, which is beyond the scope of this paper. Nevertheless, it is amply clear that there are three highly dispersive energy bands around the Γ point arising from Fe $3d$-As $4p$ hybridized states, which form three hole pockets at room temperature. This scenario is quite common in this class of materials.

2. Static ARPES data

In order to verify the sample quality and consistency of our data with the reported results [23,34], we carried out static ARPES measurements on the same sample before the trARPES measurements were done. High-quality single-crystalline $EuFe_2As_2$ samples were grown by the Sn-flux method and characterized by x-ray diffraction, Laue

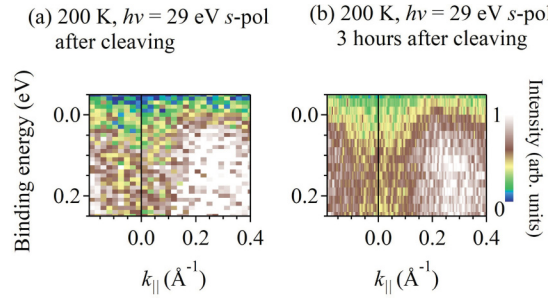

FIG. 9. Static ARPES data along the (0,0)-(π,π) direction collected at 200 K from the cleaved surface (a) immediately after cleaving and (b) 3 h after cleaving. We used s-polarized 29 eV photons and took only a few scans to ensure the sample quality without deteriorating the sample surface significantly. Both data sets look very similar and consistent with the reported results [23,34].

diffraction, and energy dispersive analysis of x rays. The sample quality was further verified by the high-resolution ARPES measurements using the photon source at the Band Dispersion and Electron-Phonon coupling (BadElPh) beamline. The quality of our ARPES data was found to be consistent with the data available in the literature [10,34]. In our trARPES experimental setup, the sample preparation chamber (base pressure of $\sim 5 \times 10^{-10}$ Torr) was used for sample cleaving to expose the clean sample surface. We transferred the sample to the preparation chamber, cleaved the sample via the top post removal method, and placed the sample into the sample analysis chamber within a moment after cleaving. For the static ARPES measurements, we used 29 eV photon energy, which is high enough to capture a large k range and is close to the k_z value of $12\pi/c$.

In Fig. 9, we show the static ARPES data for $EuFe_2As_2$ collected at 200 K; we collected only a few scans to ensure sample quality, then started time-resolved ARPES measurements so that the freshly cleaved surface was available for the time-resolved measurements without much deterioration. The experimental data exhibit signatures of α, β, and γ bands crossing the Fermi level, as expected. After detailed characterization of the sample, we used the same sample for time-resolved ARPES measurements.

[1] A. Garg, M. Randeria, and N. Trivedi, Nat. Phys. **4**, 762 (2008).
[2] C. Weber, K. Haule, and G. Kotliar, Nat. Phys. **6**, 574 (2010).
[3] A. Damascelli, Z. Hussain, and Z.-X. Shen, Rev. Mod. Phys. **75**, 473 (2003).
[4] Y. Kamihara, H. Hiramatsu, M. Hirano, R. Kawamura, H. Yanagi, T. Kamiya, and H. Hosono, J. Am. Chem. Soc. **128**, 10012 (2006).
[5] Y. Kamihara, T. Watanabe, M. Hirano, and H. Hosono, J. Am. Chem. Soc. **130**, 3296 (2008).
[6] K. Ishida, Y. Nakai, and H. Hosono, J. Phys. Soc. Jpn. **78**, 062001 (2009).
[7] F. Hardy, A. E. Böhmer, D. Aoki, P. Burger, T. Wolf, P. Schweiss, R. Heid, P. Adelmann, Y. X. Yao, G. Kotliar, J. Schmalian, and C. Meingast, Phys. Rev. Lett. **111**, 027002 (2013); G. Adhikary, D. Biswas, N. Sahadev, S. Ram, V. Kanchana, C. S. Yadav, P. L. Paulose, and K. Maiti, J. Appl. Phys. **114**, 163906 (2013).
[8] M. Yi, D. H. Lu, J. G. Analytis, J.-H. Chu, S.-K. Mo, R.-H. He, M. Hashimoto, R. G. Moore, I. I. Mazin, D. J. Singh, Z. Hussain, I. R. Fisher, and Z.-X. Shen, Phys. Rev. B **80**, 174510 (2009).
[9] M. Yi, D. H. Lu, J. G. Analytis, J.-H. Chu, S.-K. Mo, R.-H. He, R. G. Moore, X. J. Zhou, G. F. Chen, J. L. Luo, N. L. Wang, Z. Hussain, D. J. Singh, I. R. Fisher, and Z.-X. Shen, Phys. Rev. B **80**, 024515 (2009).
[10] G. Adhikary, N. Sahadev, D. Biswas, R. Bindu, N. Kumar, A. Thamizhavel, S. K. Dhar, and K. Maiti, J. Phys.: Condens. Matter **25**, 225701 (2013).
[11] G. Adhikary, D. Biswas, N. Sahadev, R. Bindu, N. Kumar, S. K. Dhar, A. Thamizhavel, and K. Maiti, J. Appl. Phys. **115**, 123901 (2014); K. Maiti, Pramana **84**, 947 (2015).
[12] L. de' Medici, G. Giovannetti, and M. Capone, Phys. Rev. Lett. **112**, 177001 (2014).
[13] T. Hajiri, T. Ito, M. Matsunami, B. H. Min, Y. S. Kwon, K. Kuroki, and S. Kimura, Phys. Rev. B **93**, 024503 (2016).
[14] M. Yi, Z.-K. Liu, Y. Zhang, R. Yu, J.-X. Zhu, J. J. Lee, R. G. Moore, F. T. Schmitt, W. Li, S. C. Riggs, J.-H. Chu, B. Lv, J. Hu, M. Hashimoto, S.-K. Mo, Z. Hussain, Z. Q. Mao, C. W. Chu, I. R. Fisher, Q. Si, Z.-X. Shen, and D. H. Lu, Nat. Commun. **6**, 7777 (2015).
[15] Z. Wang, M. Schmidt, J. Fischer, V. Tsurkan, M. Greger, D. Vollhardt, A. Loidl, and J. Deisenhofer, Nat. Commun. **5**, 3202 (2014).
[16] X. Ding, Y. Pan, H. Yang, and H.-H. Wen, Phys. Rev. B **89**, 224515 (2014).
[17] W. Li, C. Zhang, S. Liu, X. Ding, X. Wu, X. Wang, H.-H. Wen, and M. Xiao, Phys. Rev. B **89**, 134515 (2014).
[18] P. Gao, R. Yu, L. Sun, H. Wang, Z. Wang, Q. Wu, M. Fang, G. Chen, J. Guo, C. Zhang, D. Gu, H. Tian, J. Li, J. Liu, Y. Li, X. Li, S. Jiang, K. Yang, A. Li, Q. Si, and Z. Zhao, Phys. Rev. B **89**, 094514 (2014).
[19] R. Yu, P. Goswami, Q. Si, P. Nikolic, and J.-X. Zhu, Nat. Commun. **4**, 2783 (2013).
[20] B. Mansart, E. Papalazarou, M. Fuglsang Jensen, V. Brouet, L. Petaccia, L. de' Medici, G. Sangiovanni, F. Rullier-Albenque, A. Forget, D. Colson, and M. Marsi, Phys. Rev. B **85**, 144508 (2012).
[21] E. E. M. Chia, D. Talbayev, J.-X. Zhu, H. Q. Yuan, T. Park, J. D. Thompson, C. Panagopoulos, G. F. Chen, J. L. Luo, N. L. Wang, and A. J. Taylor, Phys. Rev. Lett. **104**, 027003 (2010).
[22] D. H. Torchinsky, G. F. Chen, J. L. Luo, N. L. Wang, and N. Gedik, Phys. Rev. Lett. **105**, 027005 (2010).
[23] L. Rettig, R. Cortés, S. Thirupathaiah, P. Gegenwart, H. S. Jeevan, M. Wolf, J. Fink, and U. Bovensiepen, Phys. Rev. Lett. **108**, 097002 (2012).
[24] P. Blaha, K. Schwarz, G. K. H. Madsen, D. Kvasnicka, and J. Luitz, *WIEN2K, An Augmented Plane Wave + Local Orbitals Program for Calculating Crystal Properties* (Karlheinz Schwarz, Technische Universität Wien, Vienna, 2001).
[25] P. Richard, T. Sato, K. Nakayama, S. Souma, T. Takahashi, Y.-M. Xu, G. F. Chen, J. L. Luo, N. L. Wang, and H. Ding, Phys. Rev. Lett. **102**, 047003 (2009).
[26] K. Ali, G. Adhikary, S. Thakur, S. Patil, S. K. Mahatha, A. Thamizhavel, G. De Ninno, P. Moras, P. M. Sheverdyaeva, C. Carbone, L. Petaccia, and K. Maiti, Phys. Rev. B **97**, 054505 (2018); K. Ali and K. Maiti, Sci. Rep. **7**, 6298 (2017); Eur. Phys. J. B **91**, 199 (2018).
[27] A. van Roekeghem, P. Richard, X. Shi, S. Wu, L. Zeng, B. Saparov, Y. Ohtsubo, T. Qian, A. S. Sefat, S. Biermann, and H. Ding, Phys. Rev. B **93**, 245139 (2016).

[28] Y. Zhang, F. Chen, C. He, B. Zhou, B. P. Xie, C. Fang, W. F. Tsai, X. H. Chen, H. Hayashi, J. Jiang, H. Iwasawa, K. Shimada, H. Namatame, M. Taniguchi, J. P. Hu, and D. L. Feng, Phys. Rev. B **83**, 054510 (2011).

[29] J. Fink, S. Thirupathaiah, R. Ovsyannikov, H. A. Dürr, R. Follath, Y. Huang, S. de Jong, M. S. Golden, Y.-Z. Zhang, H. O. Jeschke, R. Valent, C. Felser, S. Dastjani Farahani, M. Rotter, and D. Johrendt, Phys. Rev. B **79**, 155118 (2009).

[30] A. C. Liu, J. Stöhr, C. M. Friend, and R. J. Madix, Surf. Sci. **235**, 107 (1990); T. Hajiri, T. Ito, R. Niwa, M. Matsunami, B. H. Min, Y. S. Kwon, and S. Kimura, Phys. Rev. B **85**, 094509 (2012).

[31] C. Grazioli, C. Callegari, A. Ciavardini, M. Coreno, F. Frassetto, D. Gauthier, D. Golob, R. Ivanov, A. Kivimäki, B. Mahieu, B. Bučar, M. Merhar, P. Miotti, L. Poletto, E. Polo, B. Ressel, C. Spezzani, and G. De Ninno, Rev. Sci. Instrum. **85**, 023104 (2014).

[32] J. J. Yeh and I. Lindau, At. Data Nucl. Data Tables **32**, 1 (1985).

[33] Y. Xiao, Y. Su, M. Meven, R. Mittal, C. M. N. Kumar, T. Chatterji, S. Price, J. Persson, N. Kumar, S. K. Dhar, A. Thamizhavel, and Th. Brueckel, Phys. Rev. B **80**, 174424 (2009).

[34] S. de Jong, E. van Heumen, S. Thirupathaiah, R. Huisman, F. Massee, J. B. Goedkoop, R. Ovsyannikov, J. Fink, H. A. Dürr, A. Gloskovskii, H. S. Jeevan, P. Gegenwart, A. Erb, L. Patthey, M. Shi, R. Follath, A. Varykhalov, and M. S. Golden, Europhys. Lett. **89**, 27007 (2010); P. Richard, C. Capan, J. Ma, P. Zhang, N. Xu, T. Qian, J. D. Denlinger, G.-F. Chen, A. S. Sefat, Z. Fisk, and H. Ding, J. Phys.: Condens. Matter **26**, 035702 (2014).

[35] I. Avigo, R. Cortés, L. Rettig, S. Thirupathaiah, H. S. Jeevan, P. Gegenwart, T. Wolf, M. Ligges, M. Wolf, J. Fink, and U. Bovensiepen, J. Phys.: Condens. Matter **25**, 094003 (2013).

[36] B. Mansart, D. Boschetto, A. Savoia, F. Rullier-Albenque, A. Forget, D. Colson, A. Rousse, and M. Marsi, Phys. Rev. B **80**, 172504 (2009).

[37] J. Fink, A. Charnukha, E. D. L. Rienks, Z. H. Liu, S. Thirupathaiah, I. Avigo, F. Roth, H. S. Jeevan, P. Gegenwart, M. Roslova, I. Morozov, S. Wurmehl, U. Bovensiepen, S. Borisenko, M. Vojta, and B. Büchner, Phys. Rev. B **92**, 201106(R) (2015).

[38] M. D. Watson, A. A. Haghighirad, L. C. Rhodes, M. Hoesch, and T. K. Kim, New J. Phys. **19**, 103021 (2017); Y. S. Kushnirenko, A. V. Fedorov, E. Haubold, S. Thirupathaiah, T. Wolf, S. Aswartham, I. Morozov, T. K. Kim, B. Büchner, and S. V. Borisenko, Phys. Rev. B **97**, 180501(R) (2018).

[39] A. Rothwarf and B. N. Taylor, Phys. Rev. Lett. **19**, 27 (1967).

[40] S. L. Skornyakov, A. V. Efremov, N. A. Skorikov, M. A. Korotin, Yu. A. Izyumov, V. I. Anisimov, A. V. Kozhevnikov, and D. Vollhardt, Phys. Rev. B **80**, 092501 (2009).

[41] J. G. Analytis, R. D. McDonald, J.-H. Chu, S. C. Riggs, A. F. Bangura, C. Kucharczyk, M. Johannes, and I. R. Fisher, Phys. Rev. B **80**, 064507 (2009).

[42] S. E. Sebastian, J. Gillett, N. Harrison, P. H. C. Lau, D. J. Singh, C. H. Mielke, and G. G. Lonzarich, J. Phys.: Condens. Matter **20**, 422203 (2008).